Investigation of Nanostructured TiO_2 Surface and Interface Electric Fields with Photoreflectance Spectroscopy

Meredith C. K. Sellers and Edmund G. Seebauer
Dept. of Chemical & Biomolecular Engineering, University of Illinois at Urbana-Champaign, Urbana, IL 61801

DOI 10.1002/aic.13905
Published online August 30, 2012 in Wiley Online Library (wileyonlinelibrary.com).

The electrical properties of buried solid–solid interfaces are essential to the optimization of devices such as dye-sensitized solar cells and photocatalysts. The degree of fixed charge buildup at these interfaces can be sample-dependent, influenced by only a small fraction of total surface sites, and challenging to quantify. This work describes the applicability of photoreflectance spectroscopy (PR) to the characterization of thin film nanostructured TiO_2. The approach involves the synthesis of polycrystalline anatase TiO_2 on quartz and Si(100) by atomic layer deposition with $Ti(OCH(CH_3)_2)_4$ and H_2O as precursors. PR reveals negligible band bending at the TiO_2 free surface. A distinct spectral feature at 299.0 ± 0.3 kJ/mol (3.10 ± 0.0031 eV) is attributed to electronic states at the TiO_2-Si interface. Temporal variations in the magnitude of this feature are discussed in the context of bulk carrier concentration, solid–solid interface chemical reactions, and charge exchange between interface and grain boundary states and the bulk bands. © 2012 American Institute of Chemical Engineers *AIChE J,* 59: 1049–1055, 2013

Keywords: photoreflectance spectroscopy, anatase, atomic layer deposition, metal oxide semiconductor, TiO_2

Introduction

Conventional and photonic integrated circuits use silicon in close proximity to functional silicon oxide and nitride layers. As device length scales shrink according to Moore's Law, interfaces between these sorts of disparate materials are growing ever-closer to bulk regions. Consequently, the performance of transistors and interconnect structures are increasingly influenced by defects and fixed charge at solid–solid interfaces. Industrial-scale[1] and microfluidic[2] photocatalytic systems comprising metal oxide semiconductors like TiO_2 are similarly affected. Nevertheless, phenomena at metal oxide interfaces are comparatively less well-characterized. To further tune this class of materials for real-world applications, rates of bulk-interface charge exchange must be better understood. Additionally, metrology challenges must be overcome to allow for real-time, contactless characterization of metal oxide-substrate and metal oxide-metal junctions.

TiO_2 nanostructures have been investigated extensively for next-generation dye-sensitized solar cell (DSSC) and photocatalytic systems. In such applications, it is necessary to control electric fields near the semiconductor surface to manipulate the flow of photogenerated charge carriers. For instance, DSSCs consisting of highly ordered TiO_2 nanotube and nanorod arrays[3] exhibit enhanced charge carrier lifetime and improved photoconversion efficiency. Modeling results suggest that a built-in electric field at the TiO_2-substrate interface significantly influences DSSC performance.[4] In the context of photocatalysis, a better understanding of nanostructured TiO_2 morphology-photocurrent coupling[5] can be achieved via concurrent characterization of near-surface electric field direction and magnitude. There is even reason to believe that the dimensional anisotropy and crystallinity of TiO_2 nanotubes could[6] influence activity in the case of sulfur mustard and sarin decontamination,[7] which are mediated by near-surface hydrolysis and charge transfer reactions. Especially on large-area conductive glass substrates, where nanorod adhesion poses particular challenges, a better understanding of these interface dynamics is crucial.

There is a limited collection of techniques suitable for evaluating defects and fixed charge at solid–solid interfaces. Many, including electron beam induced current, a scanning electron microscopy (SEM) imaging mode, and electroreflectance (ER), require the formation of electrical contacts to the sample. Photoreflectance (PR) is a contactless modulation spectroscopy technique wherein a semiconductor sample is periodically perturbed with a chopped laser beam having $h\nu$ greater than the fundamental bandgap energy E_g.[8] Photogenerated minority charge carriers migrate to the interface and recombine with stored charge (Figure 1). The resulting change in built-in electric field affects the surface reflectance R in narrow regions of wavelength corresponding to optical transitions of the material under examination. The small reflectance change $\Delta R/R$ exhibits a spectral dependence that is monitored with a weaker, independent probe beam using phase-sensitive detection. The presence of a nonzero PR spectrum demonstrates unequivocally the existence of band bending.[9] The amplitude of the spectrum scales directly with the magnitude of the surface and/or interface electric field.

Importantly, modulation spectroscopy methods are well-suited to the examination of both single-crystal metal oxide semiconductors and polycrystalline semiconductors. For

Correspondence concerning this article should be addressed to E. G. Seebauer at eseebaue@illinois.edu.

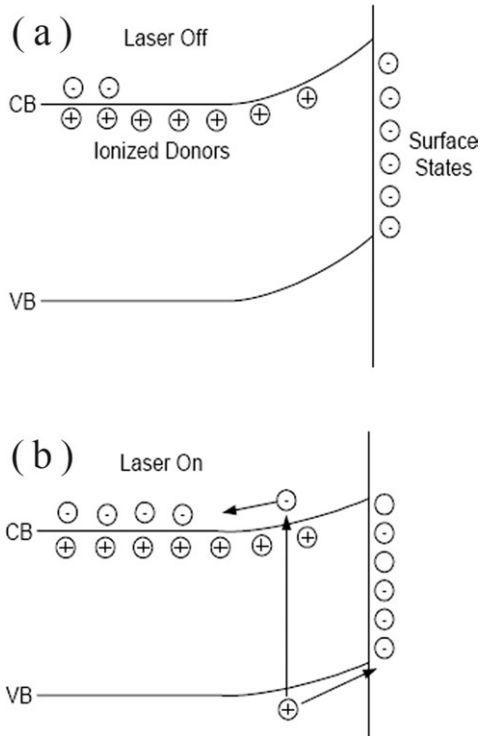

Figure 1. Schematic representation of the PR effect for a n-type sample.

When the laser is off, Fermi level pinning to surface states induces a built-in electric field. When the laser is turned on, photogenerated charge carriers recombine in the space charge region and neutralize charge in surface states.

example, ER has been used to study illuminated single crystal rutile TiO_2 (n-type, 10^{17} cm^{-3}) in contact with 0.5 M Na_2SO_4.[10] Experimentally discernible shifts in flatband voltage can be correlated to pH changes at the TiO_2-electrolyte interface and, consequently, surface state-mediated charge carrier trapping. PR spectra for single crystal ZnO exhibit the same well-defined temperature-dependent features noted for single crystal GaAs(100).[11] For polycrystalline semiconductors, grain boundaries can substantially alter film electrical properties and serve as traps for mobile charge carriers. Nevertheless, unambiguous ER spectra have been obtained for polycrystalline ZnS thin films prepared by atomic layer epitaxy at various temperatures and employing different precursor chemistries.[12] For ZnS, weaker crystallinity manifests as a broadening, rather than intensity attenuation or disappearance, of spectral features. Similar trends with respect to crystalline quality are noted for CdTe and HgCdTe[13] deposited by vacuum evaporation and CdSe[14] prepared by cathodic electrodeposition. When comparing PR spectra of β-$FeSi_2$, comparable transition energies are noted despite differences in synthesis technique and crystalline quality.[15]

This work describes the applicability of PR to characterizing metal oxide semiconductors using thin film TiO_2 as an example material. The approach involves the synthesis of thin film polycrystalline anatase TiO_2 on quartz and Si(100) by atomic layer deposition (ALD) with $Ti(OCH(CH_3)_2)_4$ and H_2O as precursors. PR is then utilized to examine surface and interface electric fields as a function of substrate type and time since film deposition.

Experimental

Preparation and characterization of polycrystalline TiO_2 films

Thin film polycrystalline anatase TiO_2 was synthesized by ALD using $Ti(OCH(CH_3)_2)_4$ and H_2O as described in Sellers and Seebauer.[16] Silicon substrates of dimensions 2 × 2 cm^2 were cut from commercial n-type Si(100) (Sb, 0.013 Ω·cm resistivity). Silicon substrates were etched with 49% hydrofluoric (HF) acid (1 min) following by rinsing with deionized water (1 min) immediately prior to insertion in the vacuum chamber to minimize native oxide formation at the TiO_2/Si interface. TiO_2 was also deposited on quartz slides that were degreased by successive 5 min rinsing cycles in electronic-grade trichloroethylene, acetone, and methanol. In both cases, the substrates were mounted on a resistively heated chuck whose temperature was maintained at 400°C during deposition and monitored with a chromel-alumel (type K) thermocouple. Film thickness was varied between 200 and 500 nm as needed by manipulation of number of ALD cycles. Films deposited at 400°C were not subjected to any post-deposition annealing. For complimentary investigation of Si substrate PR signal contributions, films were also deposited at 200°C. In some cases, these films were thermally annealed for 24 h at 550°C (ambient atmosphere) to induce crystallization.

Film thickness was measured by a Rudolph Technologies AutoEL III single wavelength ellipsometer. Film morphology was observed using a Hitachi Model S4800 SEM. The X-ray diffraction (XRD) patterns were obtained at room-temperature with a high-resolution Philips X'Pert diffractometer (λ = 0.15406 nm) operated at 45 kV and 40 mA with a Cu Kα1 primary X-ray beam from a hybrid monochromator consisting of a parabolic X-ray mirror and a 2-reflection Ge(220) monochromator. The secondary optics consisted of a high-speed PIXcel line detector using 255 channels.

PR

A schematic diagram of the experimental PR setup is shown in Figure 2. UV-grade fused silica optics were used for both the pump and probe beam optical trains; these act as filters for the pump beam photons to prevent saturation of the detector. Monochromatic light was directed through two plano-convex lenses and focused on the sample at a 45° angle of incidence. The beam was expanded horizontally by a lens with focal length of 200 mm and diameter of 50 mm (Melles Griot, LUP-50.0-93.9-UV); vertical expansion was accomplished by a lens with focal length of 175 mm and diameter of 50 mm (Melles Griot, LUP-50.0-82.2-UV). The illuminated area of the sample was approximately 1.7 × 1.7 cm^2 after beam expansion. An additional plano-convex lens (Melles Griot, LUP-50.0-82.2-UV) was inserted after the sample mount to focus the reflected probe beam onto a photodiode (Hamamatsu, S1336-44BK). The pump beam was a light-emitting diode (LED) (375 nm wavelength, Nichia Corporation, NSPU510CS) whose output was converged into a beam approximately 5 mm in diameter using a fused silica plano-convex lens with focal length of 300 mm (Melles Griot, LUP-50.0-140.9-UV). The penetration depth of the LED light beam into the TiO_2 film was calculated to be about 1000–1500 nm.

PR spectra were all acquired at room-temperature and atmospheric pressure using a LabVIEW interface for monochromator control and $\Delta R/R$ signal collection. Wavelength was scanned over the range of 425–325 nm, or near the

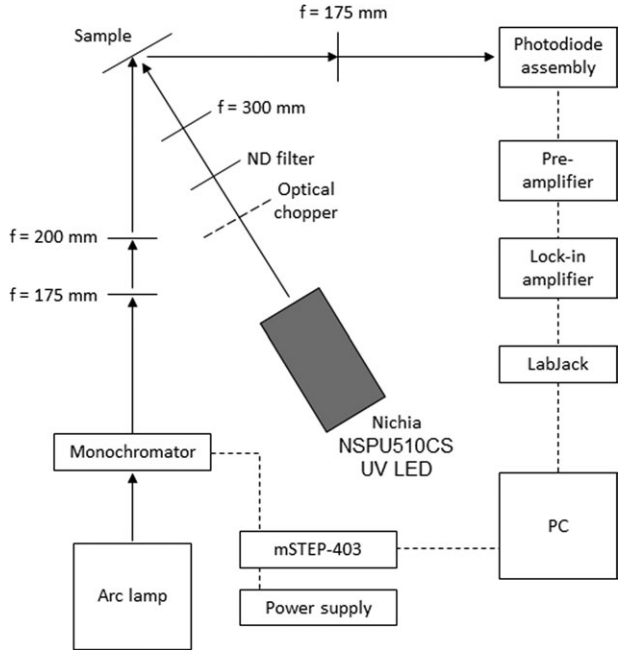

Figure 2. Schematic diagram of TiO_2 PR apparatus.

degenerate E_1 and E_0' optical transitions of Si and the fundamental band edge of anatase TiO_2 (E_g = 310 kJ/mol or 3.2 eV[17]). The monochromator was stepped at a rate of 0.15 nm/s. Between two and four different samples were examined for each distinct TiO_2/quartz and TiO_2/Si film thickness, deposition temperature, and surface pretreatment configuration.

Results

TiO_2 morphology and crystallinity

Morphology and crystallinity for a typical 500 nm polycrystalline anatase TiO_2 film deposited on quartz and Si(100) at 400°C are shown in Figure 3. As seen in the cross-sectional SEM image (Figure 3a), the film comprises high aspect ratio columnar rods approximately 45–50 nm in width with distinct spacing in between rods. The pyramidal tips of the features are easily discernible in a top view of the same film (Figure 3b). The 400°C TiO_2 film deposited on quartz is comparable in structure (data not shown). A similar morphology is observed for 1.2 μm thick TiO_2 grown on sapphire (100) by chemical vapor deposition (CVD) with $Ti(OCH(CH_3)_2)_4$ and O_2 precursors.[18]

The room-temperature XRD spectrum in Figure 3c reveals that the TiO_2 film deposited at 400°C is polycrystalline anatase, with peaks corresponding to the (101), (112), (200), and (211) orientations. Data were fit to JCPDS card No. 21-1272 (tetragonal, a = 3.7852, c = 9.5139). There is no indication of rutile (JCPDS card No. 21-1276) TiO_2. For example, analysis of the TiO_2 on Si(100) peak profile using a size-only fitting model yields an average crystallite size in the film growth direction of 43.3 ± 2.7 nm. A film strain of 0.26% was estimated by comparing the c-axis lattice constant to that of bulk anatase TiO_2. Nanostructured TiO_2 on Si(100) prepared by pulsed laser deposition (PLD) (650°C) consists of both anatase and rutile phases.[19] For PLD, the low laser fluence that spurs the evolution of rod-like features also favors the formation of anatase TiO_2.

PR spectra: TiO_2 free surface

Figure 4a shows the averaged room-temperature PR spectrum for polycrystalline anatase TiO_2 deposited on quartz at 400°C. The individual PR scans contributing to the averaged spectrum are shown in Figure 4b. In all cases, the lack of spectral features indicates negligible band bending at both the TiO_2 free surface and the TiO_2-quartz interface. This suggests that the Fermi level at the surface and within the near-surface bulk coincide, resulting in little or no electric field at the free surface. A lack of electric field would reduce the PR signal to zero.

Here, the negligible surface electric field for polycrystalline anatase TiO_2 on quartz is attributed to the passivation of dangling bonds by ambient species such as water or hydroxyls. Recent density functional theory and molecular dynamics simulations shed light on electron transfer dynamics at the H_2O-TiO_2 interface.[20] On the anatase TiO_2 surface, Zhao and coworkers have determined that competitive H_2O—H_2O and H_2O—TiO_2 interactions alter the stability of adsorbed water molecules in a coverage-dependent fashion. Unsaturated Ti and O atoms serve as electron pair donors and acceptors, in that order. Gradients in the ordering of near-surface water layers alter the electric field at the H_2O-TiO_2 interface. This phenomenon manifests experimentally in surface photovoltage and infrared spectra for water-decorated

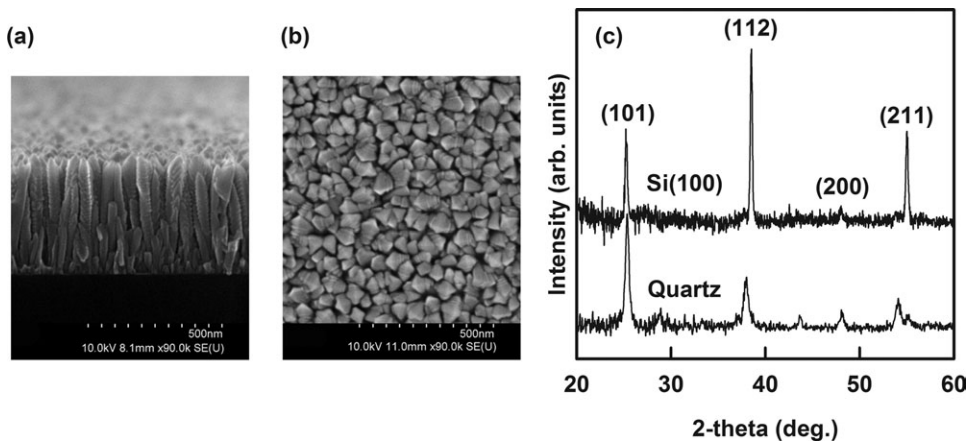

Figure 3. (a) Typical cross sectional, and (b) top view SEM images of 500 nm TiO_2 on Si(100) deposited at 400°C by ALD as well as (c) XRD data for the same film on quartz, and Si(100) with (101), (112), (200), (211) anatase TiO_2 reflections labeled (JCPDS card No. 21-1272).

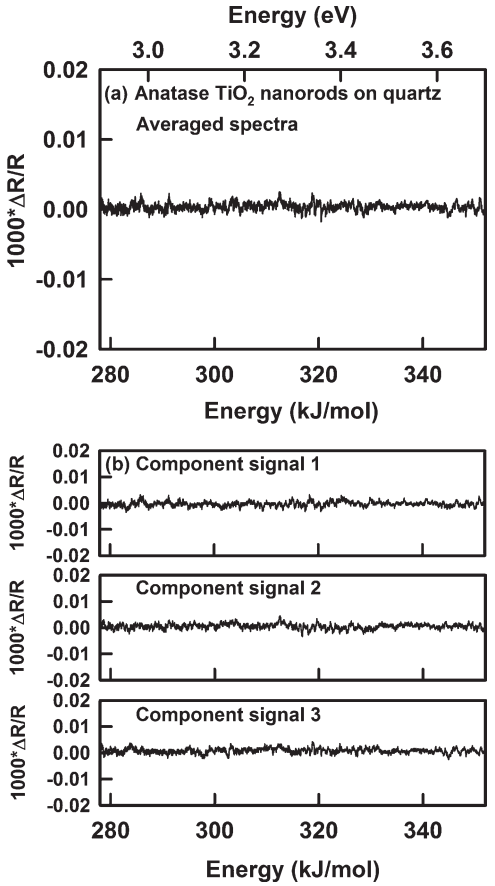

Figure 4. (a) Averaged PR spectra for 200 nm polycrystalline anatase TiO_2 on quartz deposited at 400°C, and (b) raw PR spectra for the same film.

anatase TiO_2.[21] Warren et al. note that adsorbed H_2O species affect both the magnitude and direction of the H_2O-TiO_2 interface electric field via surface-mediated charge carrier trapping.

PR spectra: TiO_2/Si interface

In contrast to the spectra presented in Figure 4a, PR data obtained for TiO_2 on Si exhibit a well-defined spectral feature, the amplitude of which decays gradually over time. Figure 5a displays typical averaged PR spectra for a 500 nm TiO_2 film on Si(100) where data is collected 1 day and 7 days after deposition. At the 1-day mark, a clear spectral feature is noted in the 294–304 kJ/mol (3.05–3.15 eV) range. The amplitude of the PR signal decreases noticeably with time to roughly one third its original value. No further signal damping is observed after the 7-day mark. Also of note, there is no evidence of a contribution from the underlying Si substrate, which would manifest as a signal at approximately 330 kJ/mol (3.4 eV).[9] Less than 9.6 kJ/mol (0.1 eV) separates the nearly degenerate E_1 and E_0' optical transitions for Si that occur at this wavelength.

Additional transient time scales are identified in TiO_2 PR spectra. The individual PR scans contributing to the averaged "day one" spectrum presented in Figure 5a are shown in Figure 5b. The four numbered runs were collected sequentially over the course of about 1 h. Less than a minute passed in between the conclusion of one run and the commencement of another. No adjustments were made to the UV LED or lock-in amplifier over the data collection period. While the PR lineshape remains fairly constant from run-to run, it inverts in a fashion that suggests the optical signal is moving from in-phase with the reference phase to 90° out of phase, to 180° out of phase, and so forth. Furthermore, there is a modest evolution in the absolute magnitude of the signal over the ~ 10 min required to collect a single spectrum.

Discussion

Lineshape for anatase TiO_2 on silicon

For polycrystalline anatase TiO_2 deposited on Si(100) by ALD, electric fields at the TiO_2-Si interface lead to non-negligible band bending at an energy substantially lower than the direct band gap[22] for TiO_2. Nevertheless, the lack of obvious Franz–Keldysh oscillations in the PR lineshape suggests that the spectrum is likely in the low-field regime.[23] For this case, a third-derivative functional form can be

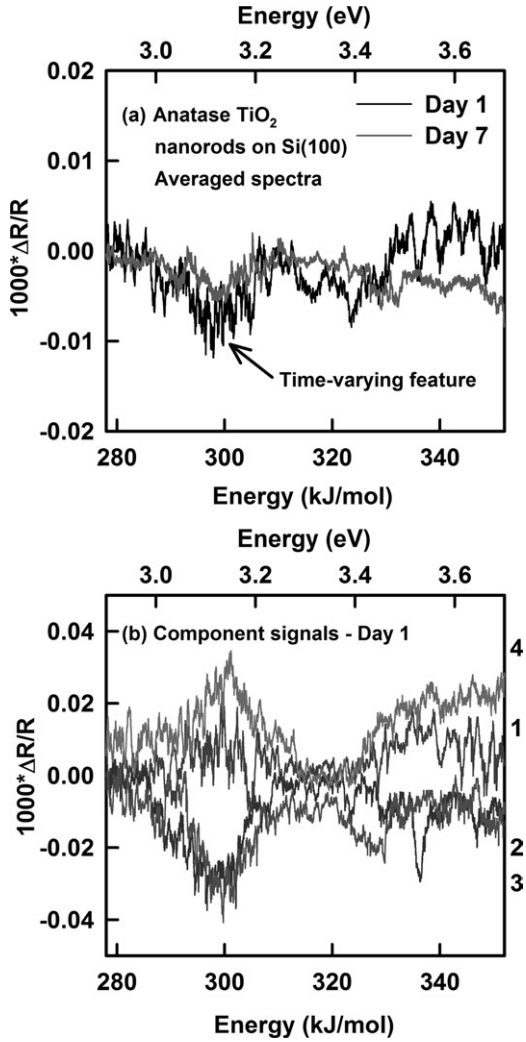

Figure 5. (a) Averaged PR spectra for 500 nm polycrystalline anatase TiO_2 on Si(100) deposited at 400°C.

In both cases, the resulting spectra comprise four runs collected sequentially over the course of about 1 h. (b) Raw PR spectra for the same film showing fast transient effects. The time sequence of PR runs is indicated by numbers 1–4 on the right side of the graph.

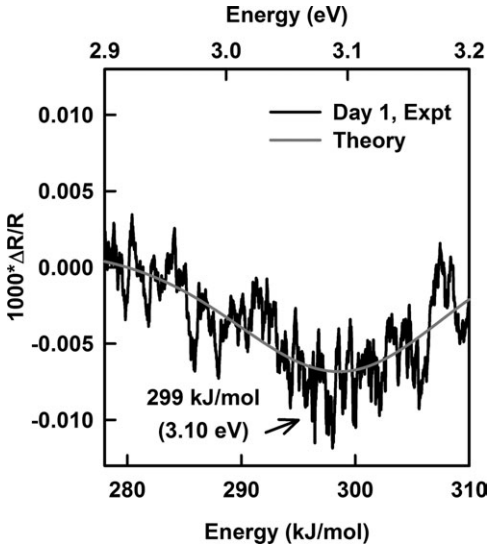

Figure 6. Comparison of day one PR spectrum from Figure 5a with theoretical low-field expression of Eq. 1.

For this spectrum, the parameters derived from Eq. 1 are $C = 1.62 \times 10^{-7}$, $\theta = 53.5°$, $\Gamma = 21.2$ kJ/mol (0.224 eV), and $E_g = 299$ kJ/mol (3.10 eV).

invoked to interpret modulation spectroscopy data. As outlined by Aspnes, the complex resonance lineshape adheres to

$$\frac{\Delta R}{R} = Re\left[Ce^{i\theta}\left(E - E_g + i\Gamma\right)^{-n}\right] \quad (1)$$

where C denotes an amplitude factor, θ a phase factor, Γ a phenomenological broadening parameter, and E_g and n the energy and dimension of the critical point associated with the transition. The formalism is equally applicable to the analysis of polycrystalline semiconductor PR and ER signals, and has been successfully invoked to fit spectral features for $FeSi_2$,[15] ZnS,[12] and ZnO.[24]

The most intense (i.e., initial) spectrum in Figure 5a was fit to Eq. 1 using a non-linear least-squares fitting routine based on a modified Marquardt-Levenberg algorithm (Figure 6). Values of $n = 2.0$, 2.5, and 3.0 correspond to the first-derivative discrete exciton and third-derivative three- and two-dimensional simple parabolic critical points, in that order.[25] Consequently, $n = 2.5$, suitable for describing general three-dimensional critical points, was used to fit the TiO_2 lineshape in this study. E_g and Γ are equal to 299.0 $\pm$ 0.3 kJ/mol (3.10 $\pm$ 0.0031 eV) and 21.2 $\pm$ 0.2 kJ/mol (0.224 $\pm$ 0.0020 eV), respectively. The detailed interpretation of these fitting parameters and their correspondence to crystal structure, wave vector, and electric field vector remains challenging for polycrystalline semiconductors.

Available ER data suggests that the feature at 3.10 eV in the PR spectrum arises from interface and grain boundary electronic states at the TiO_2-Si junction rather than the direct bandgap of anatase TiO_2. For comparison purposes, Boschloo et al.[26] used ER to examine 200 nm polycrystalline anatase TiO_2 deposited on indium tin oxide using CVD. At 0 V bias, they identified a critical point of 370 kJ/mol (3.8 eV) with a broadening factor of 20 kJ/mol (0.2 eV) that they ascribed to a direct optical transition of anatase TiO_2. Their values and feature assignment agrees well with the 368 $\pm$ 1.4 kJ/mol (3.811 $\pm$ 0.015 eV) direct gap of anatase TiO_2 determined using thermoreflectance.[22] On the other hand, Kulak et al.[27] obtained ER spectra for 100 nm films of amorphous (300°C annealing), anatase (450°C annealing), and mixed anatase-rutile (700°C annealing) TiO_2 prepared by hydrolysis of poly(butyl titrate). Annealing induced an intense signal in the sub-bandgap range of 230–290 kJ/mol (2.4–3.0 eV); the prominent spectral feature was attributed to localized surface and grain boundary electronic states.

The existence of band bending at the solid–solid interface is supported by photovoltage-based studies of TiO_2 on fluorine-doped tin oxide (FTO), Pt, and Si(100). For example, Wei et al.[28] performed transient photovoltage measurements of nanoporous TiO_2 films on FTO electrodes and semitransparent Pt substrates. A thick layer of TiO_2 (15,000 nm) was prepared by sol-gel process and annealed at 450°C to induce crystallization. At the interface between the TiO_2 film and the substrate, separation and transport of photoinduced charge carriers was controlled by a built-in electric field, the magnitude of which varied with the work function of the FTO vs. Pt substrate. Rothschild et al.[29] used surface photovoltage spectroscopy to study $\sim$ 200 nm TiO_2 on Si(100) subjected to a 24 h heat treatment in reducing ($\sim 1 \times 10^{-7}$ Pa, 450°C) or oxidizing (atmosphere, 400°C) environment. In both cases, they noted surface and intergranular interface band bending; the degree of band bending was enhanced for the oxidized film. This behavior was attributed to the chemisorption of charged oxygen atoms during the atmospheric pressure annealing process. According to the authors, states at crystallite surfaces as well as intergranular interfaces (i.e., grain boundaries) capture conduction band electrons, producing depletion layers in the adjacent regions and altering surface and intergranular potential barriers.

Transient time scales in TiO_2 PR spectra

In this study, the reduction in TiO_2 PR signal amplitude seen in Figure 5a suggests a decrease in interfacial electric field over time. This could arise due to a gradual change in bulk donor carrier concentration (N_d), a slow interfacial reaction leading to a variation in interface band bending, or charge exchange between interface and grain boundary states and the bulk bands. In the context of the experimentally determined PR spectra, a reduction in N_d would cause a widening of the space charge region and lessening of the interface electric field, even with constant band bending. Alternatively, the attenuation of the PR signal over time could arise due to a slow chemical reaction at the anatase TiO_2-Si interface, causing a decrease in band bending. Changes in microstructure or local inhomogeneity could influence spectral appearance,[13] although those explanations are unlikely here. The TiO_2 films in this study were stored at room-temperature in between successive PR examination; no variation in crystallite size or lattice strain with respect to time was discernible from repeated XRD characterization. Film thickness and elemental composition were uniform across 2 $\times$ 2 cm^2 samples; in addition, the PR signal obtained from a given sample was spatially invariant.

If a slow chemical reaction was, indeed, occurring at the TiO_2-Si interface, one might expect to see a spectral contribution from the silicon substrate appear over time. For reference, Figure 7 shows that a silicon-derived signal is visible under certain experimental conditions. When TiO_2 is deposited on Si(100) at 200°C and annealed at 550°C (to induce crystallization to bulk-like anatase TiO_2), a small silicon feature at $\sim$ 330 kJ/mol ($\sim$ 3.4 eV) is discernible in the PR

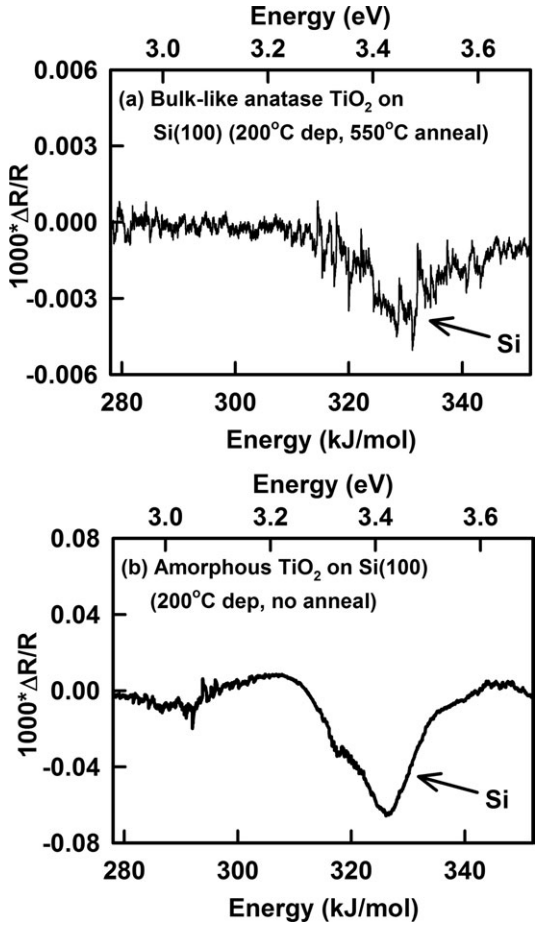

Figure 7. Averaged PR spectra showing ability to see contributions from Si substrate under some substrate preparation/film synthesis conditions where (a) is 175 nm anatase TiO_2 on Si (200°C deposition, 550°C annealing), and (b) is 450 nm amorphous TiO_2 on Si (200°C deposition, no annealing).

Native oxide was left on the Si(100) surfaces prior to TiO_2 deposition.

spectrum (Figure 7a). The silicon feature is even more pronounced in the PR spectrum for amorphous TiO_2 on Si(100) (Figure 7b). Two conclusions can be gleaned from this data. First, despite the subtle differences in film preparation method, there is every reason to believe that the UV LED is capable of generating a Si signal. No such signal is identifiable in Figure 5a, regardless of measurement acquisition interval. Second, as these particular films were deposited without HF etching of the Si substrate prior to ALD, failure to remove native SiO_2 at the Si substrate surface actually increases the degree of band bending at the interface.

By extension, it is more likely that a slow chemical reaction at the TiO_2-Si interface would lead to increased oxide formation and, thus, increased band bending. The TiO_2-Si interface for CVD films deposited at 300 and 400°C consists of a SiO_x and $TiSiO_x$ interlayer on the order of 2 nm thick.[30] A similar interlayer should exist for the films deposited at 400 and 200°C in this study. If anything, post-deposition annealing should lead to the formation of additional SiO_2 at the TiO_2-Si interface.[31] However, the decrease in PR signal observed here is uninfluenced by post-deposition annealing.

In considering the additional transient scales apparent in Figure 5b, the inversion of the PR lineshape can be explained in terms of charge exchange between defects and optically generated charges. The spectral inversion implies a phase shift of about 180° in the lock-in detection. With knowledge of the chopping frequency, the approximate time constant of this process can be estimated. As the chopping frequency is approximately 400 Hz, charge exchanges into defects at 1/400 Hz or about 2–3 ms.

For intermediate time scales, the repeatedly observed change in the absolute magnitude of the PR signal may arise from either:

1. A change in the relative contributions of two separate, but spectrally unresolved, surface state and bulk features or
2. Discharging of an interface state feature. In this case, photostimulation is responsible for both the original charging of the interface state feature and the subsequent discharging of the same feature.

Evidence to this effect stems from ER spectra of hydrogen peroxide terminated n-type, single crystal GaAs(100) in solution.[32] Koper and coworkers identified two distinct contributions to their ER spectra: one having to do with field modulation in the space charge layer and the other, a direct spectral manifestation of surface states. Modulation frequency studies revealed that surface states could not keep up with modulation greater than 200 Hz; above this frequency, the direct surface state contribution to the ER spectrum disappeared. To some degree, the broad surface state feature observed sloping upward at approximately 190 kJ/mol (2.0 eV) resembles the broad feature in Figure 5a. For the case of TiO_2 examined with the present PR configuration, it may not be possible to deconvolve surface state features from bulk features.

Conclusion

The degree of fixed charge buildup at metal oxide surfaces and interfaces can be difficult to characterize. PR, a contactless modulation spectroscopy technique, is well-suited to understanding the dynamical behavior of electric fields in nanostructured metal oxide semiconductors for DSSCs, photocatalysts, and hazardous compound remediation. Especially for high-aspect ratio structures with large specific surface areas, adsorbates capable of passivating dangling bonds may inhibit tuning of photogenerated charge carrier flow. The strong coupling between substrate type and orientation and nanoparticle, nanowire, and nanotube morphology underscores the importance of characterizing near-interface electric fields, which may exhibit temporal variations that evolve on multiple time scales. Additional effort must be devoted to unraveling the correlation between bulk TiO_2 electrical properties and electric fields at buried TiO_2-Si interfaces.

Acknowledgments

This work was carried out in part at the Center for Microanalysis of Materials at the Frederick Seitz Materials Research Laboratory, University of Illinois, which is partially supported by the U.S. Department of Energy (DE-FG02-07ER46453 and DE-FG02-07ER46471) and by the National Science Foundation. The authors acknowledge funding from the National Science Foundation through a Graduate Research Fellowship (Dr. Meredith Sellers) and Grants DMR 07-04354 and 10-05720. They would like to recognize the technical contributions of Faisal Nasim and Dr. Arshad Bhatti at the COMSATS Institute for Information Technology. Lastly, they are grateful for the assistance of Dr. Mauro Sardela, Dr. Richard Haasch, and Edmond Chow.

Literature Cited

1. Marugan J, Van Grieken R, Alfano OR, Cassano AE. Optical and physicochemical properties of silica-supported TiO_2 photocatalysts. *AlChE J*. 2006;52:2832–2843.
2. Lindstrom H, Wootton R, Iles A. High surface area titania photocatalytic microfluidic reactors. *AlChE J*. 2007;53:695–702.
3. Mor GK, Shankar K, Paulose M, Varghese OK, Grimes CA. Use of highly-ordered TiO_2 nanotube arrays in dye-sensitized solar cells. *Nano Lett*. 2005;6:215–218.
4. Ruhle S, Cahen D. Electron tunneling at the TiO_2/substrate interface can determine dye-sensitized solar cell performance. *J Phys Chem B*. 2004;108:17946–17951.
5. Thimsen E, Biswas P. Nanostructured photoactive films synthesized by a flame aerosol reactor. *AlChE J*. 2007;53:1727–1735.
6. Yun HJ, Lee H, Joo JB, Kim W, Yi J. Influence of aspect ratio of TiO_2 nanorods on the photocatalytic decomposition of formic acid. *J Phys Chem C*. 2009;113:3050–3055.
7. Prasad GK, Mahato TH, Singh B, Ganesan K, Srivastava R, Kaushik MP, Vijayraghavan R. Decontamination of sulfur mustard and sarin on titania nanotubes. *AlChE J*. 2008;54:2957–2963.
8. Cardona M. Modulation spectroscopy of semiconductors. *Festkorperprobleme* 1970;X:125–173.
9. Ditchfield R, Llera-Rodriguez D, Seebauer EG. Semiconductor surface diffusion: nonthermal effects of photon illumination. *Phys Rev B: Condens Matter*. 2000;61:13710–13720.
10. Tafalla D, Pujadas M, Salvador P. Direct measurements of flat-band potential shifts under illumination of the semiconductor-electrolyte interface by electrolyte electroreflectance. *Surf Sci*. 1989;215:190–200.
11. Seebauer EG. Oxidation and annealing of GaAs (100) studied by photoreflectance. *J Appl Phys*. 1989;66:4963–4972.
12. Lahtinen JA, Lu A, Tuomi T, Tammenmaa M. Effect of growth temperature on the electronic energy band and crystal structure of ZnS thin films grown using atomic layer epitaxy. *J Appl Phys*. 1985;58:1851–1853.
13. Amirtharaj PM, Pollak FH, Waterman JR, Boyd PR. Electrolyte electroreflectance study of laser annealing effects on the CdTe/$Hg_{0.8}Cd_{0.2}Te$(111) system. *Appl Phys Lett*. 1982;41:860–862.
14. Silberstein RP, Pollak FH, Lyden JK, Tomkiewicz M. Optical determination of Fermi-level pinning using electroreflectance. *Phys Rev B: Condens Matter*. 1981;24:7397–7400.
15. Terai Y, Noda K, Hashimoto S, Fujiwara Y. Photoreflectance study of B-$FeSi_2$ epitaxial films grown by molecular beam epitaxy. *J Phys: Conf Ser*. 2009;165:012023.
16. Sellers MCK, Seebauer EG. Measurement method for carrier concentration in TiO_2 via the Mott-Schottky approach. *Thin Solid Films*. 2011;519:2103–2110.
17. Yin W-J, Chen S, Yang J-H, Gong X-G, Yan Y, Wei S-H. Effective band gap narrowing of anatase TiO_2 by strain along a soft crystal direction. *Appl Phys Lett*. 2010;96:221901.
18. Chen C, Chen YM, Korotcov A, Huang YS, Tsai DS, Tiong KK. Growth and characterization of well-aligned densely-packed rutile TiO_2 nanocrystals on sapphire substrates via metal-organic chemical vapor deposition. *Nanotechnology*. 2008;19:075611.
19. Walczak M, Papdopoulou EL, Sanz M, Manousaki A, Marco JF, Castillejo M. Structural and morphological characterization of TiO_2 nanostructured films grown by nanosecond pulsed laser deposition. *Appl Surf Sci*. 2009;255:5267–5270.
20. Zhao Z, Li Z, Zou Z. Structure and properties of water on the anatase TiO_2(101) surface: from single-molecule adsorption to interface formation. *J Phys Chem C*. 2012;116:11054–11061.
21. Warren DS, Shapira Y, Kirsch H, McQuillan AJ. Apparent semiconductor type reversal in anatase TiO_2 nanocrystalline films. *J Phys Chem C Lett*. 2007;111:14286–14289.
22. Ho C-H, Tsai M-C, Wong M-S. Characterization of indirect and direct interband transitions of anatase TiO_2 by thermoreflectance spectroscopy. *Appl Phys Lett*. 2008;93:081904.
23. Aspnes DE. Third-derivative modulation spectroscopy with low-field electroreflectance. *Surf Sci*. 1973;37:418–442.
24. Kudrawiec R, Misiewicz J, Wachnicki L, Guziewicz E, Godlewski M. Contactless electroreflectance of ZnO layers grown by atomic layer deposition at low temperature. *Semicond Sci Technol*. 2011;26:075012.
25. Aspnes DE, Rowe JE. High-resolution interband-energy measurements from electroreflectance spectra. *Phys Rev Lett*. 1971;27:188–190.
26. Boschloo GK, Goossens A, Schoonman J. Photoelectrochemical study of thin anatase TiO_2 films prepared by metallorganic chemical vapor deposition. *J Electrochem Soc*. 1997;144:1311–1317.
27. Kulak AI, Kokorin AI, Sviridov DV. Electrolyte electroreflectance study of TiO_2 films modified with metal nanoparticles. *J Mater Res*. 2001;16:2357–2361.
28. Wei X, Xie T, Xu D, Zhao Q, Pang S, Wang D. A study of the dynamic properties of photo-induced charge carriers at nanoporous TiO_2/conductive substrate interfaces by the transient photovoltage technique. *Nanotechnology*. 2008;19:275707.
29. Rothschild A, Levakov A, Shapira Y, Ashkenasy N, Komem Y. Surface photovoltage spectroscopy study of reduced and oxidized nanocrytalline TiO_2 films. *Surf Sci*. 2003;532-535:456–460.
30. Cho YS, Heo JS, Kim JC, Moon SH. Monitoring of an interlayer between Si(100) and a TiO_2 layer formed during cyclic CVD. *Chem Vap Deposition*. 2006;12:659–664.
31. McCurdy PR, Sturgess LJ, Kohli S, Fisher ER. Investigation of the PECVD TiO_2-Si(100) interface. *Appl Surf Sci*. 2004;233:69–79.
32. Koper MTM, Chaparro AM, Tributsch H, Vanmaekelbergh D. Electrolyte electroreflectance study of the oscillatory hydrogen peroxide reduction on n-GaAs. *Langmuir*. 1998;14:3926–3931.

Manuscript received May 11, 2012, and revision received Aug. 3, 2012.